Postprocessing and Corrections of Bathymetry Derived from Sidescan Sonar Systems: Application with SeaMARC II

Pierre Cervenka and Christian de Moustier, *Member, IEEE*

***Abstract*— A procedure for postprocessing bathymetry data provided by a phase-measuring sidescan sonar system is presented. The data were collected with the SeaMARC II system, and are generally characterized by a high level of noise and uneven spatial sampling. Before any spatial filtering is applied, data are selected to remove most of the obvious artifacts and to retain instantaneous depth profiles whose slant ranges increase monotonically from a central location to the edges of the swath. An extrapolation scheme, patterned after a potential field, is proposed to fill gaps in the coverage or to extend the bathymetric swath to that of the corresponding sidescan image when regridding the data to a rectangular frame. To fill the near nadir gap typically found in these data, a specific interpolation methodology is developed that takes into account the slant range of the first bottom return as received by the sidescan sonar itself or by a shipboard echo-sounder. Spatial low-pass filtering is applied through convolutions with parabolic windows whose width is proportional to the footprint of the acoustic beam along track and roughly 1/8 of the swath width across track. Mismatches of contour lines between adjacent tracks are reduced through a statistical method designed to correct systematic athwartship profile errors.**

I. Introduction

CONVENTIONAL sidescan sonar systems provide information about the seafloor through the amplitude of the backscattered echoes they receive from the bottom; these data are usually displayed as an acoustic image of the seafloor. Over the past 20 years, several sidescan sonars have been developed with the additional ability to measure the phase difference of echoes received at two or more rows of transducers on each side of the sonar package. Bathymetry is then obtained by determining the range and elevation angle of bottom reflectors in the athwartships plane, using interferometric methods or by direct analysis of the phase difference between signals arriving at adjacent rows (e.g. [1]–[5]). In addition, coregistered bathymetric and backscatter amplitude data share the same spatial properties in the reference frame of the sonar, so that an ideal system can potentially deliver integrated information [6]: e.g., relative echo strength draped over a 3-D representation of the bottom relief, or a map of bottom scattering strength in geographic coordinates, without the need to combine data from different sonar systems [7]–[10].

Here, we are concerned with postprocessing the bathymetry data derived from phase measuring sidescan sonar systems. The goal is to create reliable contour maps of the topography of the area surveyed, or to provide a representation of the seafloor relief that is usable in subsequent geometric corrections of the images of backscatter amplitude (e.g., [7], [10]). Although these processing methods have been developed using data collected with the SeaMARC II system, most of them can be implemented with data collected by other bathymetric sidescan sonar systems.

For SeaMARC II, there is a single pair of acoustic arrays per side, with about half a wavelength separation between the rows of a pair. In the real-time processing operations leading to the tape recorded digital data that we use here, for each ping, raw base-banded quadrature samples of the received echoes are converted to instantaneous phase difference values that are binned in a 2D histogram of phase versus time. Then, the mode of the time histogram for each phase difference bin is selected to form a sequence of differential phase versus time [4], [11]. This sequence is often noisy, and it usually contains instances of synchronous phase difference angles that are ambiguous in a sidescan geometry. Factors such as loss of correlation between the signals received at each transducer row in a pair, due, for instance, to decreased signal-to-noise ratio, multipath interference, or specular reflections, all contribute to noise in the phase sequence. Further uncertainties are introduced during the conversion of electrical phase angles to elevation angles in the athwartships plane. As in most bathymetric sidescan sonars, an empirical look-up table is used in SeaMARC II for this conversion. For a patch of seafloor whose depths is representative of the general survey area, and whose relief is presumed flat across the swath, a table is generated by matching measured arrival times with computed straight-line slant ranges to the flat bottom. Such a table is valid over a limited depth range because it accounts for the acoustic geometry as well as for refraction effects due to changing sound speed in the water column. Consequently, the more the bottom topography changes from the representative depth used to compute the table, the more systematic biases are introduced in the bathymetry during the angle conversion process [4]. These angular uncertainties and those related to the dynamics

Manuscript received June 18, 1993; revised May 23, 1994. This work was supported by the Office of Naval Research under Grants N00014-91-J-1073 and N00014-90-J-4009 under management by the Marine Physical Laboratory and the Hawaii Institute of Geophysics, respectively.

P. Cervenka was with the Marine Physical Laboratory, Scripps Institution of Oceanography, La Jolla, CA 92093 USA. He is now with the Laboratoire de Mécanique Physique, Université Paris VI, 78210 Saint Cyr l'Ecole, France.

C. de Moustier was on leave at the Naval Research Laboratory, Washington, DC. He is with the Marine Physical Laboratory, Scripps Institution of Oceanography, La Jolla, CA 92093 USA

IEEE Log Number 9403706.

of the sonar platform are mainly responsible for higher levels of variance in the bathymetry data [12].

In this paper, we describe a number of post processing techniques intended to select, filter, and correct such noisy bathymetry data. In their preprocessed form, these data are referenced within the athwartship plane, on a ping-by-ping basis. Thus, for each ping, the system must provide information on the status, the geographical position, and the attitude of the sonar platform. However, seafloor surveys are usually performed along a pattern of more or less straight tracks. During the straight runs, we assume that the heading of the sonar platform is nearly steady (actual yaw amplitude is about 1° on straight runs), and that the interval between pings is almost constant (a manual switch setting in SeaMARC II). Hence, we consider the bathymetry as the representation of a surface built with data spread over successive parallel lines, each line corresponding to one ping. When the yaw amplitude of the platform exceeds the azimuthal width of the beam pattern of the sonar, or when ping intervals are irregular, subsequent steps must be taken to account for the resulting deformation of the spatial representation of the bottom. However, such operations are not addressed here.

In Section II, we describe the process by which bathymetry data recorded by SeaMARC II are selected and tested for consistency. The sequence of operations required to filter these data along and across track, as well as the extrapolation and interpolation techniques used to regrid the data on rectangular matrices, are presented in Section III. SeaMARC II does not produce bathymetry in a sector roughly 20° to 30° wide centered on nadir, where differential phase measurements are unreliable. To help bridge this gap and form a bathymetric profile that is continuous athwartships, we present in Section IV an interpolation scheme that takes into account the slant range of the first echo, and the first valid depth samples on either side of nadir. Finally, a statistical method intended to reduce the bias introduced by the table look-up conversion from phase to elevation angles is described in Section V, and examples of the different processes are given.

II. Data Description and Selection

The first set of operations that must be performed on the bathymetry data involves verification and selection. For each ping, these data consist of: 1) a port and a starboard (*stbd*) sequence of depth-athwartships distance pairs ((z_i, x_i), $i = 1, n$, $x_{i\_stbd} < 0$), 2) information about the position of the sonar in the water column, given by its depth below the sea surface h_s and its altitude above the bottom h_a, and 3) a time stamp and navigation information from which the horizontal distance traveled by the sonar between pings can be inferred. In SeaMARC II data, the port and starboard bathymetric sequences are derived independently and stored in one file, along with a nadir depth value (for $x = 0$) computed by the system. A separate file contains the sonar attitude and navigation information. Both files are sequenced with one record per ping, each record including a time stamp. However during data acquisition, these files are created on different computers and the time stamps might not match exactly.

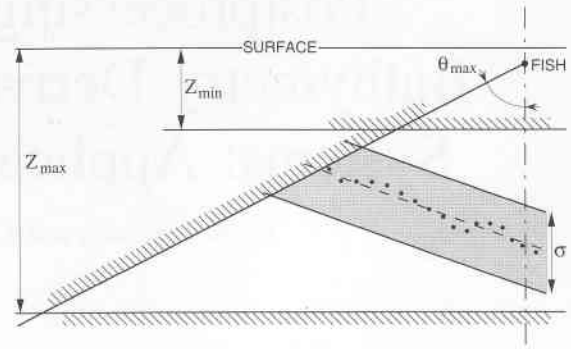

Fig. 1. Templates used to filter each half bathymetry profile. User-specified upper z_{min} and lower z_{max} limits on depths, as well as a maximum athwartship angular sector θ_{max} serve to eliminate most outliers, and to retain data that fall within 1 σ of the linear regression of the resulting profile (stippled band).

During data verification, the attitude file is scanned for chronological order, and for consistency of the reported depth and altitude values from one ping to the next. Beyond certain reasonable limits, currently set as an absolute threshold of 10 m for the depth and a relative variation of 10% for the altitude, data are flagged and eventually replaced. Bathymetry records are then processed on a ping-by-ping basis, and their time stamps are matched to those of the attitute file with a tolerance that is short (±1.5 s) in comparison to a typical ping interval in excess of 8 s. When a bathymetric record is missing, a dummy record is inserted with the appropriate time stamp in the sequence of pings and a single data pair $(z, x) = (h_s + h_a, 0)$, corresponding to the sum of the altitude and the depth of the sonar at nadir.

The goal of the data selection stage is to remove spurious values and artifacts that might have been introduced by the real-time bathymetry processing algorithms before the data were logged. To this end, we have designed a set of templates against which the (z, x) pairs are evaluated. Data from each side are handled independently in the same way they were acquired. A first-order template consists of user-defined bounds on depth (z_{min}, z_{max}) and on the maximum angular width of the swath to one side (θ_{max}). *A priori* knowledge of the general relief to be found in the area surveyed helps in choosing the vertical limits z_{min} and z_{max}. In most cases, SeaMARC II bathymetric data are limited by the onset of bottom multiple interferences to an angular swath width of ±60° about nadir. However, data on the outer edges of this swath are often of questionable reliability because of low signal-to-noise ratio, and the template provides a way to reduce the allowable swath width through θ_{max}. Another template is automatically generated for each side by computing the linear regression of the corresponding instantaneous bathymetric profile. This defines a band centered on the mean profile (stippled area in Fig. 1), whose width is proportional to the standard deviation (e.g., $\pm 1\sigma$). Data that do not fit in these templates are simply discarded, thereby eliminating most of the obvious outliers.

A further selection process is necessary to deal with the the multiple synchronous echoes commonly found in these data. The algorithm that selects the modal time for each phase bin in the 2D phase–time histogram allows echoes arriving

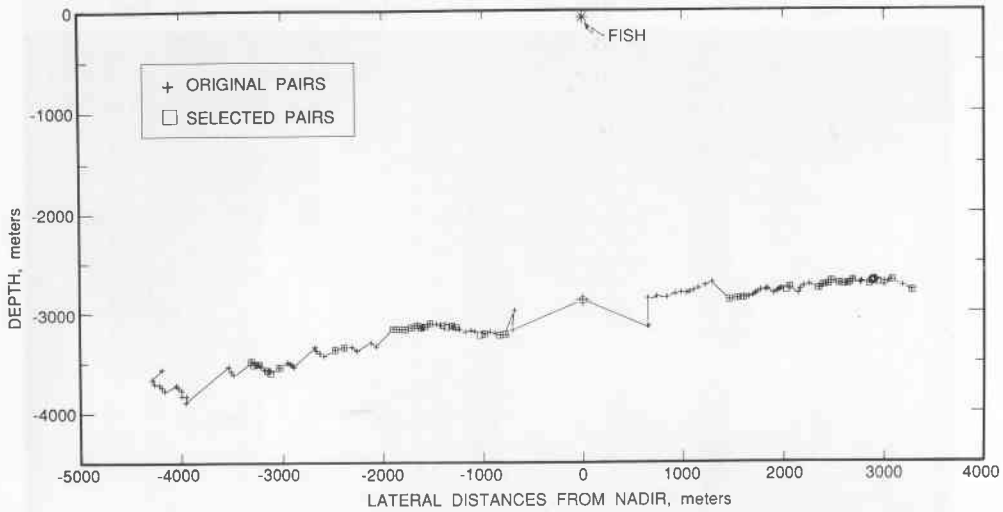

Fig. 2. Results of the data selection based on a monotonically increasing slant range with increasing athwartships elevation angle for a single ping. Only the selected data (squares) are used in subsequent processing steps. In this instance, roughly half of the original samples (+) were discarded.

at the same time from different directions to be converted to bathymetry, thus creating an across-track echelon of small concave features whose points have the same slant range. We consider such features as artifacts because the broad athwartships fan beam of a sidescan sonar cannot separate multiple synchronous echoes in the athwartships plane, and there must be a monotonically increasing relation between slant range (i.e., time) and elevation angle. By the same token, slant ranges must increase across track. For each side, the profiles are scanned from nadir outward, and data pairs whose slant range is smaller than those previously encountered are flagged. The process is applied in reverse, starting at the outer edge of the profile towards nadir, flagging points whose slant range is larger than those previously encountered in that direction. Finally, all flagged pairs are discarded, and we only retain the sequences of (z, x) pairs whose horizontal components x increases strictly monotonically with the elevation angle $\theta = \arctan[x/(z - h_s)]$:

$$x_i < x_j \Rightarrow \frac{x_i}{z_i - h_s} < \frac{x_j}{z_j - h_s}. \tag{1}$$

The distribution of data points in the bathymetric profiles resulting from this selection process is usually sparser and more uneven than in the original sequence. However, the remaining points are probably more reliable. For convenience in the processing steps to follow, we regrid them evenly into a rectangular format. This is done by median decimation of the sequence to one point per user-defined interval of angular elevation (e.g., $\Delta\theta = 1°$). Others [13] have regridded directly the raw SeaMARC II bathymetry data without going through this selection process, and then applied one-dimensional low-pass filters for noise reduction. We feel that the data selection is necessary because artifacts are likely to remain after low-pass filtering, and their spatial characteristics might be altered sufficiently to make their detection more difficult.

An example of the selection process applied to a single profile is displayed in Fig. 2, with almost no vertical exaggeration. However, to check whether the process does not throw away relief information, along-track consistency must be considered. This is illustrated in the first two panels of Fig. 3 for a continuous sequence of several hundred pings. The swath of original bathymetry data is displayed in Fig. 3(a) and the selected data are displayed in Fig. 3(b). The only notable difference between these two figures is the attenuation, in Fig. 3(b), of spurious features that appear approximately parallel to the track in Fig. 3(a).

III. Rectangular Format

Selected (z, x) pairs from both sides of the swath are regridded in a single rectangular matrix, one row per ping [Fig. 4(a)]. This format is convenient for subsequent bidimensional processing. The total width of the rectangle, $2x_s$, is chosen to match the swath width of the backscatter amplitude data, e.g., about 10 km with Sea MARC II. Although the corresponding bathymetric swath is usually smaller, extrapolating it to the edges of the image swath provides a basis to perform geometric corrections on the backscatter image as described elsewhere [7], [10].

For each row i, four parameters characterize the inner and outer edges of the data available on port and starboard; $x\_stbd_{\max}[i]$, $x\_stbd_{\min}[i]$, $x\_port_{\min}[i]$, and $x\_port_{\max}[i]$. Over a number of consecutive pings, the shape of these boundaries is very uneven, especially on the outer edges. To produce a more evenly filled rectangular gird, new regularly spaced values are interpolated between $x\_stbd_{\max}[i]$ and $x\_port_{\max}[i]$. The exterior areas $x_{\max}[i], x_s]$ are then filled by extrapolation from end members $\{(z, x)_{\max}\}$ of nearby rows that are "visible" from the end of the current row. This procedure is illustrated in Fig. 4(b) when the datum to be extrapolated is at the end of row j on port side, at an athwartships distance x such that

$$0 < x_{\max}[j] < x \leq x_s. \tag{2}$$

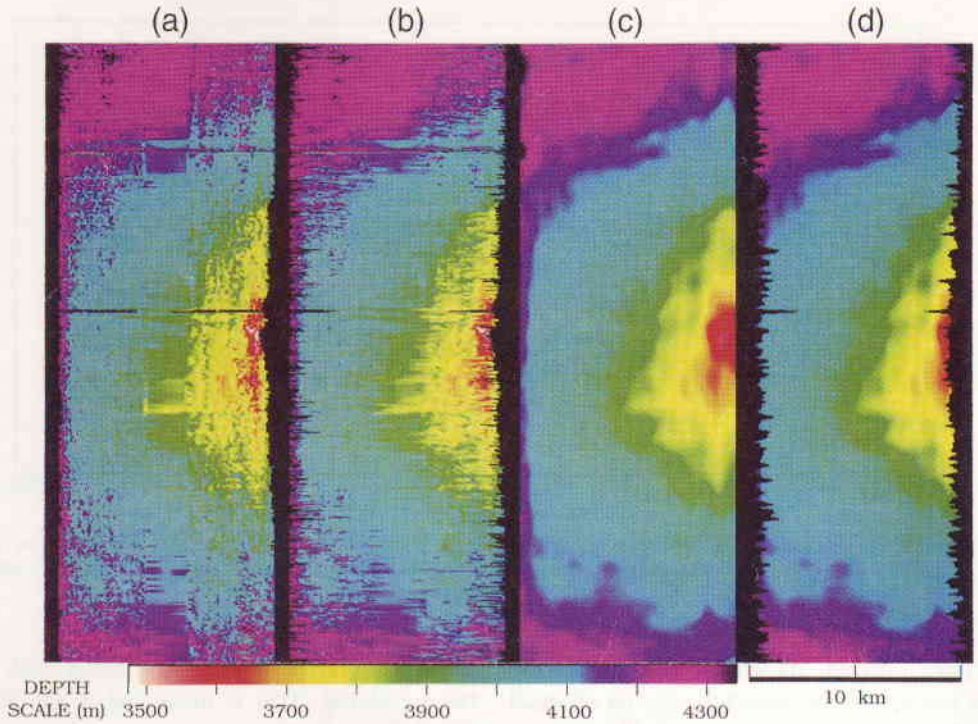

Fig. 3. Results of the data selection and filtering processes for a contiguous series of pings. The color scale extends from about 3500 m (pink) to 4300 m (violet), and the swaths are roughly 10 km wide. (a) Initial representation of the bathymetry as provided by the Sea MARC II system. The central area is interpolated between port and starboard, using the system computed nadir value if available. (b) Selected (z, x) pairs with the same nadir interpolation as in (a). (c) Bathymetry obtained with the selected data of (b), after gridding, interpolation near nadir using the slant range of the first bottom return, extrapolation from the outer edges of the original swath to the rectangular boundaries, and low-pass filtering along and across track. (d) Same as (c), but cropped to the boundaries of the selected data shown in (b).

The corresponding depth value is computed from the weighted sum:

$$z(x) = \frac{\sum_i \frac{z(x_{\max}[i])}{l_{ij}^2(x)}}{\sum_i \frac{1}{l_{ij}^2(x)}} \tag{3}$$

with

$$l_{ij}^2(x) = (i-j)^2 \Delta p^2 + (x - x_{\max}[i])^2$$

where Δp is the average along-track distance traveled between successive pings. The weighting process mimics a potential field in that the influence of a datum decreases with the square of its distance from the extrapolated point. Practically, the summation is limited to neighboring pings, i.e, $|i-j|\,\Delta p \leq x_s$. In addition, only data that can be "seen" from the extrapolation datum are taken into account. Therefore, $x_{\max}[i]$ is included in (3) if there is no masking data between pings i and j, i.e.,

$$(i-j)x_{\max}[k] < (i-k)x + (k-j)x_{\max}[i], \quad \text{whenever } (i-k)(k-j) < 0. \tag{4}$$

Once the rectangular matrix is completely filled, along-track filters can be applied. In keeping with the finite azimuthal resolution of the sidescan sonar system, we filter these data along track using parabolic windows whose width increases athwartships in proportion to the size of the beam footprint along track. However, although the actual azimuthal fan aperture of the sonar is around 2° at the half power point, the size of the windows is calculated with an azimuthal sector of about 10° to 12° wide to make allowances for the movements of the platform and for the uncertainty in the elevation angle measurements that contribute to noise in the bathymetry. After this operation, the bathymetry is much smoother athwartships,

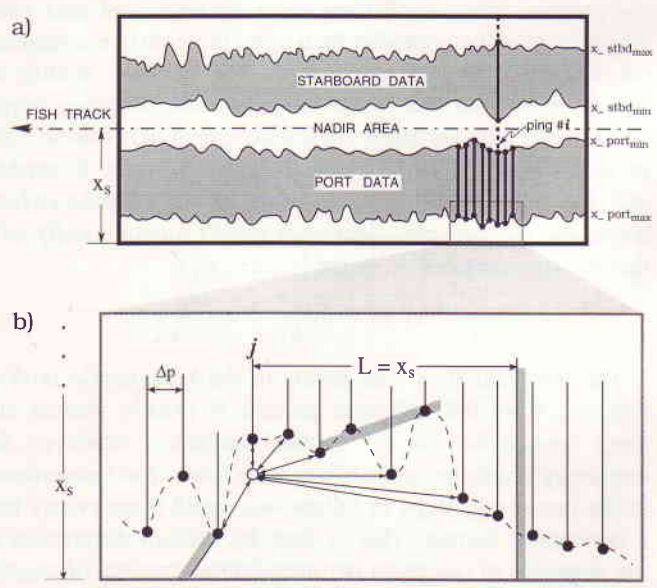

Fig. 4. (a) Rectangular format and data limits on either side of the fish track. The half swath width x_s in rectangular format is set equal to that of the image of acoustic backscatter amplitude (e.g., 5 km for most Sea MARC II data). (b) Extrapolation scheme. The point to be extrapolated on the jth ping (empty circle) is computed as a weighted sum of the visible data from other pings lying within a specified horizontal range x_s.

but there is still a noticeable discontinuity in the central portion of the swath due to the data gap about nadir. To alleviate this problem, we have devised an interpolation scheme that takes into account, for each ping, the slant range of the first detected bottom return and the first valid bathymetry points at the inner edges $x\_port_{\min}$ and $x\_starboard_{\min}$ of the profile. The details of the interpolation method are given in Section IV. This interpolation scheme must be performed after the data verification and selection stage, but it can be applied before or after the data have been regridded and filtered as described above. Here, we have chosen to apply it after the filtering process to get somewhat more stable results. Likewise, the sequence of sonar depth h_s and altitude h_a can be filtered along track before entering this interpolation algorithm.

The extrapolation and along-track filtering operations are redone after the nadir interpolation process because the boundaries of the nadir region can extend deeply outward. This is achieved by rebuilding the rectangular matrix with the original preselected data augmented with the estimated central samples. The along-track filtering is then followed by across-track filtering with parabolic windows about 1/8 of the total swath width wide. This size is consistent with the expected athwartships spatial resolution of the system derived in a theoretical study [12]. The resulting bathymetry shown in Fig. 3(c) is essentially seamless, but it contains extrapolated data that we might not want to retain. To this end, the processed rectangular array is restored to the original format of (z, x) pairs by cropping it to the low-pass filtered exterior boundaries of the selected data [Fig. 3(d)]. As seen in this figure, the output of these processes is a sequence of bathymetric profiles, with a greatly reduced noise content, which can be machine contoured once merged with navigation data [14].

IV. Near Nadir Profile Estimation

A. Geometry of the Problem

Within the confines of a directional beam, the intersection of a spherically radiating acoustic pulse with the bottom is first an ellipse rapidly changing to a portion of annulus [15]. Hence, images of seafloor acoustic backscatter amplitude delivered by sidescan sonars typically do not include the nadir area because, under the flat bottom assumption, this region yields strong specular returns that tend to saturate the receivers. Likewise, phase measurements are unreliable in this region because of constructive and destructive interferences of the signals backscattered by the elemental areas of the pulse footprint near normal incidence. As a result, bathymetry data are available only beyond a certain lateral angle from nadir, typically around 10° to 15°. In addition, the first echo arrives from the closest bottom area seen by the sonar at normal incidence. So unless the bottom is flat and horizontal, the nadir depth value, estimated by adding the depth of the fish and its altitude computed from the first echo arrival, is usually incorrect and it introduces along-track artifacts in the representation of the seafloor relief.

The motivation for adequate interpolation across the central gap is to alleviate boundary concerns in subsequent data processing steps: spatial filtering is much easier to implement, and the port and starboard swaths can be connected with reasonable and smooth contour lines. The simplest method to estimate the geometry at nadir consists of interpolating linearly between the first valid data points on port and starboard. As mentioned earlier, although this solution is generally acceptable, it tends to leave a noticeable discontinuity in the profile. The technique we use here achieves better results by including the slant range of the first bottom return in the solution.

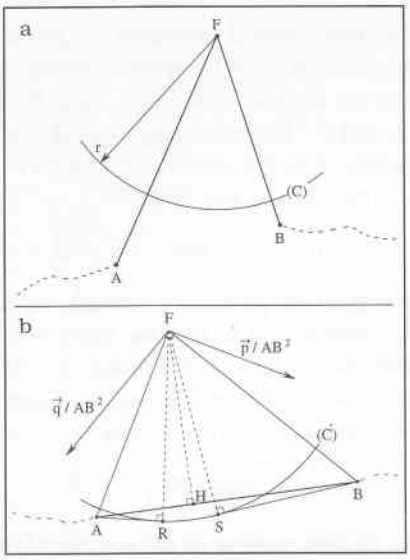

Fig. 5. (a) Geometry of the near nadir interpolation problem. A and B are the first valid bathymetry samples on either side of nadir; the radius r of circle (C) is the slant range of the first bottom return. (b) Geometry of the near nadir interpolation when circle (C) intersects $]AB[$ and the solution is the arc segment RS. The near nadir profile is concave.

The geometry of the problem can be limited to the athwartships plane because the narrow azimuthal width of the sidescan sonar beam pattern (typically 2°) constrains the patch of seafloor that returns the first bottom echo to the athwartship plane. In this plane, the blind portion of the profile is bounded by the first reliable bathymetric data available on either side of nadir [points A and B in Fig. 5(a)] after the selection and verification stages described in Section I. The data selection ensures that these points bound nonambiguous portions of the profile, and that the slant ranges are strictly increasing when following these profiles outward. Consequently, these points must surround the portion of profile from where the first echo originated. Assuming that the minimal slant range r of the profile is known, the locus of the first reflector(s) seen by the sonar is the arc of circle (C) of radius r centered at the fish location F, limited by the sector (FA, FB).

The goal is to produce the simplest and most reasonable near nadir profile that can be supported by this set of data $\{F, A, B, r\}$. This involves assigning the first arrival to an appropriate location P on the arc of circle (C), and then completing the profile by linear interpolations out to the known boundaries A and B. Because the amount of information available is very limited, it seems logical to require that the choice of P result in a bottom profile as smooth as possible.

B. Solutions

In this section, special attention is given to providing practical formulas that can be applied directly with the set of parameters given in their basic form: r and the coordinates of points F, A, and B. The processing algorithm must first check for incompatible data, for which one or both of the following slant range conditions is not verified:

$$r \leq FA \quad \text{and} \quad r \leq FB. \tag{5}$$

Then, according to the guidelines previous stated, the location of point P is determined so that the angle it defines with the adjacent interpolated parts of the profile is maximized.

The simplest situation to resolve occurs whenever circle (C) intersects the segment $]AB[$, yielding

$$\overrightarrow{FA} \cdot \overrightarrow{FB} < FH^2 < r^2 \tag{6}$$

where H is the intersection of the segment with the perpendicular line drawn from F [Fig. 5(b)], and FH^2 is evaluated using the law of sines in triangle FAB:

$$FH^2 = d^2/AB^2, \qquad \text{with } d^2 = FA^2FB^2 - (\overrightarrow{FA} \cdot \overrightarrow{FB})^2. \tag{7}$$

A natural and simple way to describe the near nadir profile is to consider the arc RS of circle (C), linked with the segments $[AR]$ and $[BS]$. Points R and S are derived from the straight tangent lines drawn from points A and B to circle (C). In order to write an explicit form for the location of R and S, it is convenient to define vectors $\vec{p}$ and $\vec{q}$:

$$\vec{p} = FA^2\overrightarrow{FB} - (\overrightarrow{FA} \cdot \overrightarrow{FB})\overrightarrow{FA} \tag{8a}$$

$$\vec{q} = FB^2\overrightarrow{FA} - (\overrightarrow{FA} \cdot \overrightarrow{FB})\overrightarrow{FB} \tag{8b}$$

which are perpendicular to $\overrightarrow{FA}$ and $\overrightarrow{FB}$, respectively, and such that

$$\overrightarrow{FH} = (\vec{p} + \vec{q})/AB^2. \tag{9}$$

Using the length d as defined in (7) yields

$$\overrightarrow{FR} = \frac{r}{FA^2}\left[r\overrightarrow{FA} + \left(\frac{FA^2 - r^2}{d^2}\right)^{1/2}\vec{p}\right] \tag{10a}$$

$$\overrightarrow{FS} = \frac{r}{FB^2}\left[r\overrightarrow{FB} + \left(\frac{FB^2 - r^2}{d^2}\right)^{1/2}\vec{q}\right] \tag{10b}$$

Here, the solution is not a single point P, but the whole arc RS, and the profile angles at points R and S are the largest possible, i.e., 180°. A solution that uses two straight segments $[PA]$ and $[PB]$ linked by a single point P would violate the initial assumptions because part of these segments would necessarily lie at a slant range smaller than r.

Whenever the conditions written in (6) do not hold but (5) is verified, a single point P can be found so that angle $(\overrightarrow{PA}, \overrightarrow{PB})$ is maximized and the slant range of any point belonging to segment $[AP[\cup]PB]$ remains strictly larger than r. Simple geometric considerations show that this result is obtained with the intersection of circle (C) with one of the two tangent circles (C') that pass through points A and B. However, as mentioned previously, this solution must lie within the sector (FA, FB).

Looking at the limit case drawn for one side in Fig. 6(a), this condition requires that the center of circle (C') lie on FA or FB. Using the original set of data, this means that the point where circles (C) and (C') are tangent is outside the sector (FA, FB) if one of the following conditions is true:

$$r\overrightarrow{FA} \cdot \overrightarrow{AB} > |FA|\overrightarrow{FB} \cdot \overrightarrow{AB} \tag{11a}$$

or

$$r\overrightarrow{FB} \cdot \overrightarrow{AB} < |FB|\overrightarrow{FA} \cdot \overrightarrow{AB}. \tag{11b}$$

These conditions are exclusive. Using (5), it can be shown that (11a) implies $\overrightarrow{FA} \cdot \overrightarrow{AB} < 0$, and point P is set so that the angle $(\overrightarrow{PA}, \overrightarrow{PB})$ is as open as possible, i.e., taking P at the intersection A' of line FA with circle (C) [Fig. 6(b)]:

$$\overrightarrow{FP} = \frac{r}{FA}\overrightarrow{FA} \tag{12a}$$

On the other side, when (11b) is verified, $\overrightarrow{FA} \cdot \overrightarrow{AB} > 0$, and we take $P = B'$:

$$\overrightarrow{FP} = \frac{r}{FB}\overrightarrow{FB}. \tag{12b}$$

In both cases, the near nadir bottom profile is modeled by the segments $[AP] \cup [PB]$.

Finally, when neither (6) nor (11a), (11b) is true but (5) is, one must find the intersection P of the tangent circles (C) and (C'). This amounts to solving the following set of equations, in which Q is the point diametrically opposed to P in (C') [Fig. 6(c)]:

$$\overrightarrow{AP} \cdot \overrightarrow{AQ} = 0 \tag{13a}$$

$$\overrightarrow{BP} \cdot \overrightarrow{BQ} = 0 \tag{13b}$$

$$\overrightarrow{FQ} = a\overrightarrow{FP}, \qquad a > 1. \tag{13c}$$

For any a, there are two solutions. The first is given by the circle (C'), exterior to (C), such that (disk $C') \cap (C) = P$, whereas the other is a circle containing (C) completely and is irrelevant. This choice implies that coefficient a in (13c) must be larger than unity. From a practical point of view, it is important to realize that the analytical derivation for the location of P must be done carefully because artificial poles are easily introduced in the solution.

To proceed in the derivation, it is convenient to define two orthogonal vectors $\vec{u}$ and $\vec{v}$:

$$\vec{u} = -(FB^2 - r^2)\overrightarrow{FA} + (FA^2 - r^2)\overrightarrow{FB} \tag{14a}$$

$$\vec{v} = (\vec{u} \cdot \overrightarrow{FB})\overrightarrow{FA} - (\vec{u} \cdot \overrightarrow{FA})\overrightarrow{FB} \tag{14b}$$

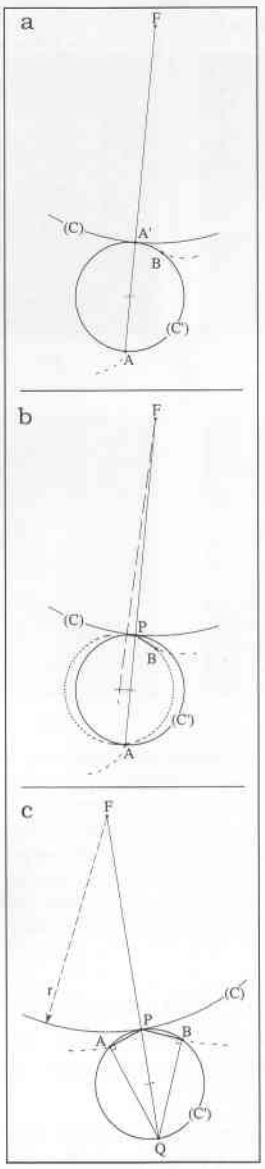

Fig. 6. Limit cases of the position of the first bottom reflector with respect to sector AFB. (a) Limit case to one side, the center of circle (C') lies on FA. (b) the center of circle (C') (dashed line) lies outside FA, and the solution is forced to circle (C') (solid line) going through A and whose center lies on FA. (c) Example of the geometry resulting in a convex profile in the near nadir area.

so that the final result can be explicitly written as

$$\overrightarrow{FP} = r\left(\frac{r(FA^2 - FB^2)}{u^2}\vec{u} + \left(\frac{AB^2(FA^2 - r^2)(FB^2 - r^2)}{u^2v^2}\right)^{1/2}\vec{v}\right), \quad (15)$$

which is a very robust form to compute when both (6) and (11) are not verified. The profile is again modeled by the segments $[AP] \cup [PB]$. In this case, the location for P yielding the flattest possible angle $(\overrightarrow{PA}, \overrightarrow{PB})$ is unique.

All the situations that can be encountered are summarized in Fig. 7. Given data points A and B and the slant range r of the first bottom echo, this diagram maps various domains for

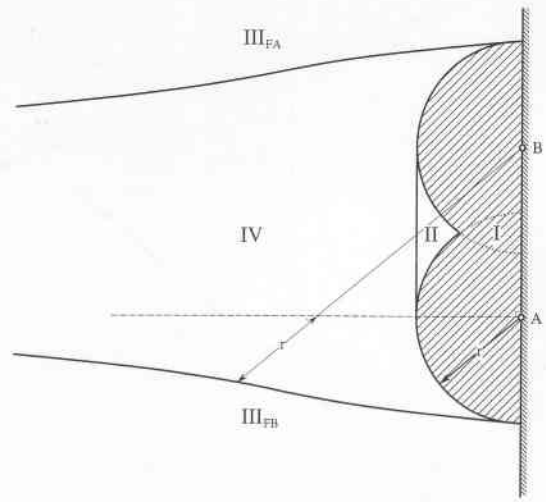

Fig. 7. Map of regions of validity for the solutions of the near nadir interpolation problem. A and B are the available bathymetric data closest to nadir. r is the slant range to the closest reflector. The location of the fish with respect to these points dictates which solution applies.

the location of point F. Zone I corresponds to incompatible data, i.e, (5) is violated. Zone II is the location of F where (6) applies, leading to the solution depicted in Fig. 5(b). Zones III$_{FA}$ (11a) and III$_{FB}$ (11b) delimit the areas for which P must be kept on either side of sector (FA, FB) [(12a) and Fig. 6(b), (12b)]. Such cases are seldom encountered in the data, but they are implemented here mainly to improve the robustness of the algorithm. Zone IV bounds the most usual location of F for which (15) applies [Fig. 6(c)].

The transition between Zones II and IV is a special case where the value of r is equal to the distance between the fish and the straight line AB, so that (6) becomes

$$\overrightarrow{FA} \cdot \overrightarrow{FB} < FH^2 = r^2. \quad (16)$$

In that case, (10a), (10b), (15) all give the same result, equal to $\overrightarrow{FH}$ given in (9):

$$\overrightarrow{FR} = \overrightarrow{FS} = \overrightarrow{FP} = \overrightarrow{FH}. \quad (17)$$

Hence, the proposed model fits here with the most intuitive solution, where P is located on the segment $[AB]$, which represents the estimated profile.

The complete algorithm, with a simplified version of the treatment in Zone II, has been implemented in a real-time bathymetry processing software package that was successfully tested with recorded SeaMARC II raw acoustic data. So, it can potentially be used on line during data acquisition at sea.

We have assessed the performance of this interpolation method with simulated topography and a sonar geometry representative of Zone IV. The data were created by navigating a fictitious sonar, with spatial sampling characteristics similar to those of SeaMARC II, at an altitude of 2800 m above a symmetric ridge (Fig. 8). The geometric parameters of this simulation have been exaggerated to magnify the distortions created by the different interpolation algorithms at nadir. The slopes of the ridge are 45° and the track crosses the crest line at an angle of 45°. The blind zone at nadir is set to

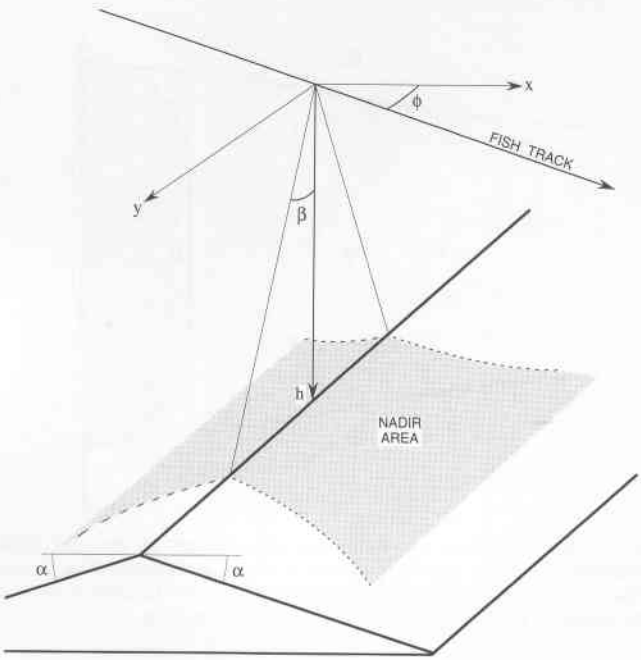

Fig. 8. Geometry of a simulated flight over a ridge. The fish track is oblique (ϕ) to the ridge crest line, the blind zone near nadir (stippled) is delimited by the angle 2β, and α is the slope of the symmetric ridge. In this example, $\phi = 45°$, $\beta = 22.5°$, and $\alpha = 45°$.

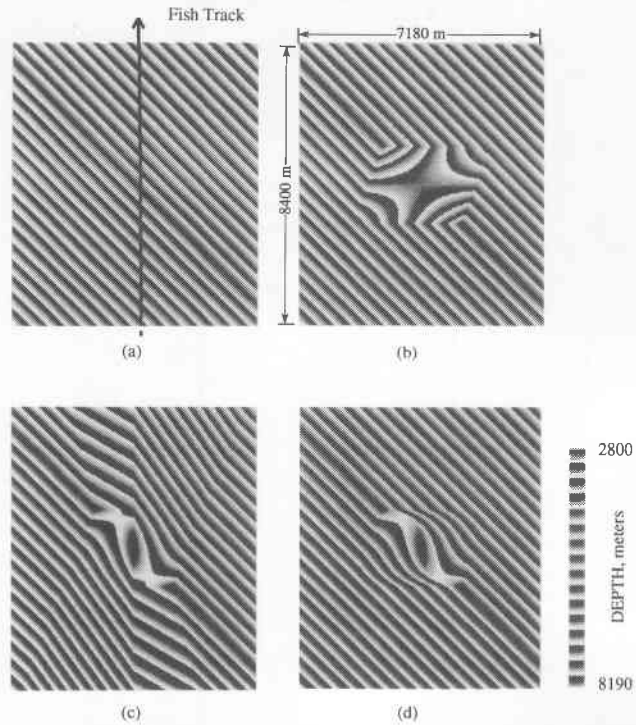

Fig. 9. Bathymetric representation of a ridge using: (a) simulated relief, (b) reconstruction of the relief with straight line interpolation between bathymetric samples obtained with the sonar, (c) reconstruction of the relief where the slant range of the first echo return is used as a vertical sounding in the interpolation between samples near nadir, (d) near nadir interpolation using the proposed algorithm that estimates a nadir depth based on the slant range of the first echo return and the valid bathymetry data point nearest nadir on either side. In all cases, the depth increment per fringe of gray tones (black to white) is 337.5 m.

a large half width of 22.5°. The original simulated ridge and three bathymetric renditions by the sonar are presented in Fig. 9(a)–(d), where depth contours are displayed as gray level fringes covering a depth interval of 337.5 m each. In Fig. 9(b), an interpolation was performed across the nadir blind zone without taking into account the slant range of the first return. A saddle developed in the resulting bathymetry at the crest of the ridge, due to straight line interpolation between points on opposite flanks of the ridge. When the slant range of the first return is interpreted as a measurement of the depth directly below the fish, the bathymetric representation of the crest is somewhat improved [Fig. 9(c)]. However, as discussed in Section IV-A, this method introduces other artifacts on the flanks where a spurious ridge has been created along the fish track. Although the restoration is not perfect, a marked improvement is obtained after application of our nadir interpolation algorithm [Fig. 9(d)], and the remaining distortions have a much smaller areal extent than those found in the other two cases.

C. First Bottom Echo Derived From Another Echo-Sounder

In theory, the nadir altitude can be derived from the echoes received by another echo-sounder, operated aboard the towing ship. Aside from the obvious spatial registration difficulties inherent in a solution involving a shipboard echo-sounder, several factors make it a less desirable solution if there is a choice. For instance, bathymetry obtained with a multibeam echo-sounder is usually very suitable, but there is often a nonconstant depth offset with the bathymetry obtained with a SeaMARC II system (e.g., [10]). Depth measurements made with a conventional 12 kHz echo-sounder, or with a 3.5 kHz subbottom profiler, might be biased by the large fore–aft beamwidth (e.g., 30°) of such a device, allowing the first return to come from outside the athwartship plane, or by the inability of that system to resolve adequately the water–sediment interface.

This problem is particularly relevant when the survey track follows the relief up-dip (e.g., Fig. 10) or down-dip. The first target seen by an echo-sounder can be anywhere in the cone delimited by the angular aperture γ of its transducer. Let s_x be the "depth" measurement obtained by the echo-sounder when the fish is in the athwartship plane Π_x, located at the along-track abscissa x. We assume that the corresponding target lies in the nadir area, on the portion of sphere of radius s_x, centered at x, limited fore and aft by the planes $\Pi_{x \pm s_x \sin\gamma}$ (Fig. 11). So if the first return is detected at range s_x, the minimal range measurable with the sidescan sonar signals in the neighboring athwartship planes $\Pi_{x \pm s_x \sin\delta}(|\delta| \leq \gamma)$ is greater than $s_x \cos\delta$. Thus, at a postprocessing stage, and provided the fish is towed along a straight and horizontal trajectory, a minimal range r_x for the equivalent sidescan target can be defined for each athwartship plane Π_x by taking the maximal projection derived from the neighboring measurements:

$$r_x = \max_{\sin|\delta| \leq \sin\gamma} \{s_{x+u} \cos\delta\}, \qquad \text{with } \sin\delta = u/s_x. \quad (18)$$

The methodology presented in Section IV-B can then be applied by using these computed r_x values.

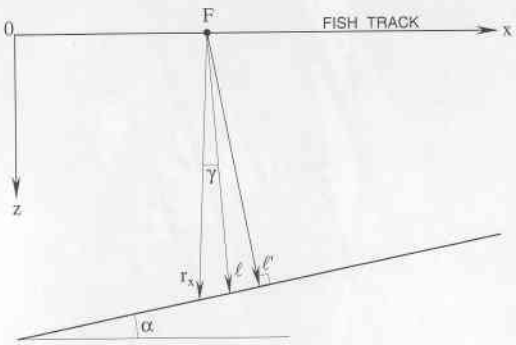

Fig. 10. Along-track profile showing the original of the first bottom echo as measured by a sidescan sonar r_x, or by an echo-sounder of half beamwidth γ over a bottom with slope α: $s_x = l$ when $\gamma \leq \alpha$, and $s_x = l'$ when $\gamma \geq \alpha$.

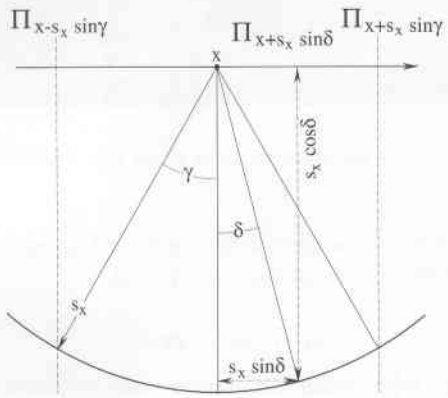

Fig. 11. Displacement of the athwartships plane Π_x when using a conventional echo-sounder of half beamwidth γ to determine the slant range s_x of the first bottom echo.

V. Processing of a Complete Survey: Correction of Systematic Biases

When combining several swaths of SeaMARC II bathymetry from a survey area into a bathymetric map, one often finds consistent mismatches of the depth values on adjacent tracks. This suggests that the athwartships profiles are biased, and that the look-up tables used to convert differential phase into elevation angles were not sufficiently accurate. As mentioned before, these errors could be due to bathymetry falling outside the range of validity of the look-up table. In addition, the sonar platform might not be completely level, or its roll sensor might be slightly offset with respect to the frame of reference of the acoustic arrays, allowing a small roll bias to exist in the tables.

This could be remedied by computing new tables and reprocessing the raw differential phase data. However, until recently, the raw quadrature samples were seldom recorded because doing so meant handling crates of nine-track magnetic tapes. In SeaMARC II, only the processed phase data output by the histogram modal picking algorithm mentioned earlier were recorded on a routine basis. Rather than compute new tables from these data that contain their own set of artifacts, we investigated ways to eliminate the biases on a statistical basis.

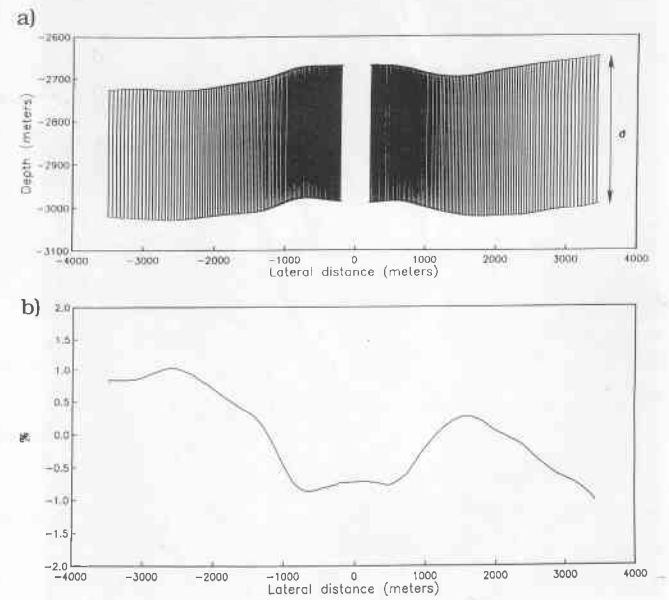

Fig. 12. Statistics derived from across-track profiles for the area shown in Fig. 13. (a) Average across-track profile and standard deviation σ centered on this average. (b) Percentage that the average profile in (a) deviates from a flat and horizontal profile at the overall average depth for the area.

Starting with bathymetry data that have been already selected through the procedures described in Section II, we choose an area whose relief is homogeneous. A statistical analysis is performed to generate a smooth average athwartships profile. This profile is then used to correct each individual datum, so that the same statistics performed on the corrected bathymetry yield a flat profile.

While scanning the attitude files, the number of samples, the cumulated fish depths h_s and altitudes h_a, and the cumulated squares of each of these parameters are stored. Likewise, while scanning bathymetry records, bathymetry data are sorted in bins of athwartships elevation angles, with a specified bin size $\Delta\theta$. Each (z, x) pair is assigned to the ith bin according to

$$\tan(i\,\Delta\theta) \leq \frac{x}{z - h_x} < \tan([i+1]\,\Delta\theta) \tag{19}$$

where h_s is found in the corresponding attitude record. Information stored in each bin includes the number of pairs, the cumulative abscissas, the cumulated water column heights, and the cumulated height squares.

The binned array is then decimated to a smooth average profile $\{(Z, X)_i\}$ with approximately uniform standard deviations [e.g., Fig. 12(a)]. The correction [Fig. 12(b)] is based on the assumption that the average profile was actually flat and horizontal, with the reference water column height Z_r equal to the sum of the average fish depth D_r and the average altitude H_r, both derived from the attitude statistics. The binned profile is transformed into a table $\{(R, T)_i\}$ that associates a corrective ratio R with the tangent of an elevation angle T:

$$T_i = \frac{X_i}{Z_i - D_r} \quad \text{and} \quad R_i = \frac{H_r}{Z_i - D_r}. \tag{20}$$

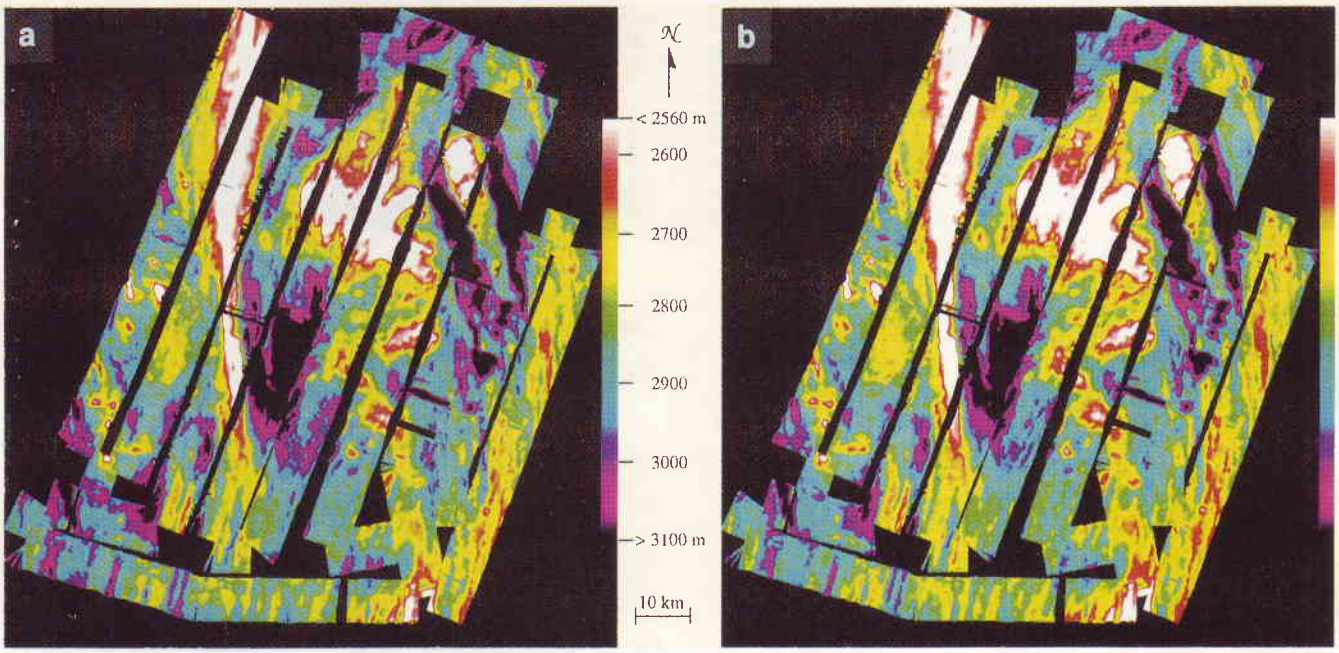

Fig. 13. Example of athwartship profile correction applied to SeaMARC II bathymetry data for a nontransform offset of the East Pacific Rise located around 36° S 111° W. (a) Before correction. (b) After correction.

Using linear interpolation to evaluate $R(T)$, each (z, x) pair is finally corrected according to

$$z \to h_s + (z - h_s)R\left[\frac{x}{z - h_s}\right]. \tag{21}$$

Data are not translated horizontally, so that the transformation performed with (21) is not strictly equivalent to changing the "flat bottom" conversion table. However, the resulting effect is quite similar. Small angular variations would affect both the horizontal and the vertical components of each datum. But the resulting horizontal changes would remain much smaller than the final horizontal resolution of the bathymetry provided by a phase-measuring sidescan sonar.

An example of this statistical bias removal procedure applied to a whole survey area is provided in Fig. 13. These data were collected with the SeaMARC II system in 1992, at a nontransform offset of the East Pacific Rise near 36° S, 111° W, between the Pacific and Antarctic plate boundaries [16]. The rise axis is the white linear feature extending north–south of the left side of the map, with its southern extension visible in the south–east corner of the survey area. The average depth in the area is 2900 m.

There are no dramatic differences between the original [Fig. 13(a)] and the "corrected" [Fig. 13(b)] representations of the relief, but edge-to-edge matching of adjacent tracks has improved (granted the reader must take our word for it because it is nearly impossible to tell at the scale of reproduction used for publication.) Most of the changes involve depths that lie on the shallow end of the depth scale (< 2700 m, yellow–red–white), suggesting that the look-up table might have been computed for a deeper depth. This can be seen in the track furthest to the east, and in the northwest corner of the survey area. Changes involving depths at the deeper end of the scale (>3000 m, purple) can also be noted in the centermost track, as well as in the southwest corner and in the central northern sector of the survey area.

VI. Conclusion

In dealing with swath bathymetry data collected with the SeaMARC II sidescan sonar system, our goal was to convert the original noisy an artifact prone data into a self-consistent set of bathymetric samples that could be easily and reliably handled by contour-mapping algorithms.

Before any kind of spatial filtering was applied to the data, we deemed it necessary to go through a selection process to eliminate most of the obvious artifacts present in the data. Although specifically developed for SeaMARC II bathymetry data, part of this selection process was based on the spatial sampling characteristics of any sidelooking sonar systems that make it impossible to resolve multiple synchronous echoes in the athwartships plane. In the same way that we have processed images of seafloor acoustic backscatter amplitude [17], spatial low-pass filters that take into account the azimuthal acoustic geometry of the sonar were applied to the selected data after they had been regridded to a uniform rectangular format. Gaps between the uneven edges of the swath and the boundaries of the rectangle, or between pings, were filled using an efficient extrapolation routine that performs a weighted sum of the "visible" neighboring data to create each new point.

A bathymetric sidescan sonar cannot produce direct measurements of the bottom profile in the nadir area. However, the width of the central gap in the bathymetric swath coverage is not much larger than the athwartships horizontal resolution that the system can deliver elsewhere. Hence, it seemed reasonable to develop an interpolation method, taking into account the slant range of the first echo return, to provide the smoothest connection possible near nadir between the port and starboard swaths of bathymetry.

Finally, we have investigated a statistical approach to correcting systematic athwartship biases in the bathymetric profiles. The procedure simulates a correction of the "flat bottom" table used by the SeaMARC II system to convert differential phase angles into athwartships elevation angles, but it requires no *a priori* knowledge of the table originally used. This method provides improved matching between isolines of adjacent swaths, making it easier for gridding and contouring applications.

Acknowledgment

We thank A. N. Shor for his support, P. Lonsdale for providing the data displayed in Fig. 13, and J. Griffith (MPL) and I. Jewett (NRL) for the artwork.

References

[1] P. N. Denbigh, "Phase only side-scan sonar for underwater mapping," *Acoust. Lett.*, vol. 1, pp. 84–87, 1977.
[2] R. L. Cloet, S. L. Hurst, C. R. Edwards, P. S. Phillips, and A. J. Duncan, "A sideway-looking towed depth measuring system," *J. Roy. Inst. Navigation,* vol. 40, pp. 9–17, 1986.
[3] J. O. Klepsvik and K. Klov, "TOPO-SSS, a sidescan sonar for wide swath depth measurements," in *Proc. Offshore Technol. Conf.*, pp. 477–487, 1982.
[4] J. G. Blackinton, "Bathymetric mapping with SeaMARC II: An elevation angle measuring side-scan sonar system," Ph.D. dissertation, Hawaii Inst. Geophys., Univ. Hawaii, Manoa, 1986.
[5] M. A. Masnadi-Shirazi, C. de Moustier, P. Cervenka, and S. H. Zisk, "Differential phase estimation with the SeaMARC II bathymetric sidescan sonar system," *IEEE J. Oceanic Eng.,* vol. 17, no. 3, pp. 239–251, 1992.
[6] C. de Moustier, M. A. Masnadi-Shirazi, and P. Cervenka, "Integrated processing for bathymetry and sidescan data in swath bathymetry sidelooking sonars," *EOS, Trans. Amer. Geophys. Union,* vol. 72, no. 44, pp. 249–250, 1991.
[7] P. Cervenka, C. de Moustier, and P. F. Lonsdale, "Pixel relocation in SeaMARC II sidescan sonar images based on gridded Sea Beam bathymetry," *EOS, Trans. Amer. Geophys. Union,* vol. 71, no. 43, pp. 1407–1408, 1990.
[8] N. C. Mitchell, "Improving Gloria images using Sea Beam data," *J. Geophys. Res.,* vol. 96, no. B1, pp. 337–351, 1991.
[9] T. K. Lau and C. G. Fox, "A technique for combining SeaMARC I sidescan sonar and gridded bathymetry data to display undistorted seafloor images," in *Proc. IEEE Oceans'91,* vol. 2, pp. 1140–1145, 1991.
[10] P. Cervenka, C. de Moustier, and P.F. Lonsdale, "Geometric correction on sidescan sonar images based on bathymetry. Application with Sea MARC II and Sea Beam data," *Marine Geophys. Res.,* to be published.
[11] H. Matsumoto, "Characteristics of SeaMARC II phase data," *IEEE J. Oceanic Eng.,* vol. 15, pp. 350–360, 1990.
[12] P. Cervenka, U. C. Herzfeld, and C. de Moustier, "Accuracy of the spatial representation of the seafloor with bathymetric sidescan sonars," *Marine Geophys. Res.,* to be published.
[13] A. Malinverno, M. H. Edwards, and W. B. F. Ryan, "Processing of Sea MARC swath sonar data," *IEEE J. Oceanic Eng.,* vol. 15, no. 1, pp. 14–23, 1990.
[14] P. Cervenka, C. de Moustier, and P. F. Lonsdale, "Corrections on SeaMARC II sidescan sonar bathymetry," *EOS Trans. Amer. Geophys. Union*, vol. 72, no. 44, p. 249, 1991.
[15] C. de Moustier and D. Alexandrou, "Angular dependence of 12 kHz seafloor acoustic backscatter," *J. Acoust. Soc. Amer.*, vol. 90, no. 1, pp. 522–531, 1991.
[16] P. F. Lonsdale, "Geomorphology and structural segmentation of the crest of the southern (Pacific-Antarctic) East Pacific Rise," *J. Geophys. Res.,* vol. 99, no. B3, pp. 4683–4702, 1994.
[17] P. Cervenka and C. de Moustier, "Sidescan sonar image processing techniques," *IEEE J. Oceanic Eng.,* vol. 18, no. 2, pp. 108–122, 1993.

Pierre Cervenka received the Doctorate degrees in acoustics and physics, both from the Pierre & Marie Curie University, Paris, in 1982 and 1988, respectively.

In 1983, he joined the Centre National de la Recherche Scientifique (CNRS) as a Research Scientist. Most of his studies were involved with nonlinear acoustics and modeling of parametric antennas. From 1989 to 1992, he was a Visiting Assistant Researcher at the Marine Physical Laboratory of the Scripps Institution of Oceanography. He is now with the Laboratoire de Mécanique Physique (Université Paris 6), where his research interests are in underwater acoustics. For photo, please see the April 1993 issue of this Journal.

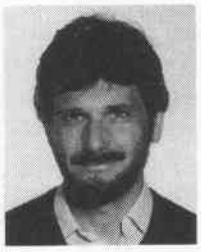

Christian de Moustier (M'86) received the Diploma of Engineer from the Ecole Supérieure d'Ingénieurs de Marseille, France, in 1979, and the M.S. and Ph.D. degrees in oceanography (applied ocean science) at the University of California, San Diego, in 1981 and 1985, respectively.

He is with the Scripps Institution of Oceanography, where he is an Associate Research Oceanographer at the Marine Physical Laboratory, and an Academic Administrator for Ship Operations and Marine Technical Support. In 1993, he was a Visiting Scientist in the Marine Physics Branch of the Naval Research Laboratory, Washington, DC. His present research interests are in underwater acoustics with emphasis on the physics of bottom-interacting sound and sound reverberation in the ocean, seafloor acoustic imaging and contour mapping, and digital image processing applied to sonar data.

Dr. de Moustier was Guest Editor of the October 1989 Special Issue of the IEEE Journal of Oceanic Engineering. Since then, he has been serving as Associate Editor for the Journal. He is a member of the Acoustical Society of America and the American Geophysical Union.